

## Article

# Structure Optimization of Longitudinal Rectangular Fins to Improve the Melting Performance of Phase Change Materials through Genetic Algorithm

Yang Xu, Hang Yin, Chen He, Yong Wei, Ming Cui and Zhang-Jing Zheng \*

School of Low-carbon Energy and Power Engineering, China University of Mining and Technology, Xuzhou 221116, China

\* Correspondence: zhengzj@cumt.edu.cn

**Abstract:** In this paper, the structural parameters of longitudinal rectangular fins used in a horizontal shell-and-tube latent heat storage unit (LHSU) are optimized to increase the melting rate of phase-change materials. The influence of natural convection on the melting process is considered. Due to the extremely nonlinear and expensive computational cost of the phase-change heat-transfer-optimization problem, a new coupling algorithm between genetic algorithm and computational fluid dynamics is developed. The effects of the thermal conductivity of fins; the filling rate of fins; and the number of fins on the optimal structure parameters, including the length, width, and position of each fin, are discussed. The results show that when a single fin is inserted in the half-ring region, the optimal dimensionless fin angle is about 0.2, and the optimal dimensionless fin length is about 0.96. The use of optimal single fin can shorten the dimensionless total melting time by 68% compared with the case of no fin, and 61.3% compared with uniformly arranged single fin. When the number of fins exceeds one, each fin should have a specific length ( $L$ ), thickness ( $\Delta$ ), and position ( $\psi$ ) instead of uniform distribution. The advantage of the optimized fins decreases as the number of fins increases. When the number of fins is four, the optimized fin distribution is almost uniform, and the dimensionless total melting time is only 15.9% less than that of the absolutely uniform fin. The number of fins is a more sensitive parameter affecting the optimal position and structure of fins than the filling rate and thermal conductivity of fins.

**Keywords:** phase-change material (PCM); melting; heat-transfer enhancement; fin; computational fluid dynamics (CFD); genetic algorithm (GA)



**Citation:** Xu, Y.; Yin, H.; He, C.; Wei, Y.; Cui, M.; Zheng, Z.-J. Structure Optimization of Longitudinal Rectangular Fins to Improve the Melting Performance of Phase Change Materials through Genetic Algorithm. *Energies* **2022**, *15*, 9610. <https://doi.org/10.3390/en15249610>

Academic Editors: Evangelos Bellos, Chao Xu, Yu Qiu and Qiliang Wang

Received: 21 October 2022

Accepted: 15 December 2022

Published: 18 December 2022

**Publisher's Note:** MDPI stays neutral with regard to jurisdictional claims in published maps and institutional affiliations.



**Copyright:** © 2022 by the authors. Licensee MDPI, Basel, Switzerland. This article is an open access article distributed under the terms and conditions of the Creative Commons Attribution (CC BY) license (<https://creativecommons.org/licenses/by/4.0/>).

## 1. Introduction

Thermal energy storage (TES) technology has a wide application in solar thermal utilization and waste heat recovery systems. Latent heat TES (LHTES) is one of the promising TES technologies, storing heat in liquid–solid phase-change materials (PCMs) in the form of latent heat. In the LHTES system, the PCM is encapsulated in the storage unit called LHTES unit. Heat is carried into and out of the LHTES unit by heat-transfer fluid (HTF). The shell-and-tube LHTES unit is a commonly used LHTES unit since it can be easily manufactured [1]. In addition, the shell-and-tube LHTES unit gives a better charging and discharging performance than rectangular LHTES unit [2]. Numerous research studies related to the shell-and-tube LHTES unit have focused on the heat-transfer enhancement to promote the charging and discharging efficiency [3–6], such as adding heat pipe [7], metal foam [8], nanoparticles [9], graphite [10], etc.

The utilization of fin is a cheap and easy-to-process strategy for heat-transfer enhancement [11,12]. In a shell-and-tube LHTES unit, HTF usually flows in the tubes, and the PCM is encapsulated in the shell. During the heat-transfer process between the HTF and PCM, the maximum thermal resistance regularly occurs in the PCM, so fins are usually fixed on the outside of the tube to enhance heat transfer in the PCM. There are two types of fins

that can be attached to the outside of the tube: longitudinal and transversal. Generally, the rectangular fin is longitudinal, and the ring fin is transversal. This paper concerns the longitudinal rectangular fins, and the research progress is summarized as follows.

The research of the longitudinal fin with a rectangular shape can be divided into two stages according to the arrangement of fins. In the first stage, the fins are evenly arranged. Some research of the first stage focused on verifying the thermal strengthening effect of the rectangular fins and revealing the melting and solidification characteristics under the influence of the fins. Rabienataj Darzi et al. [13] compared the melting and solidification performances of a double-tube LHTES unit enhanced by adding longitudinal rectangular fins and using an elliptical inner tube instead of a round inner tube through the numerical method. Twelve longitudinal rectangular fins with fixed structural parameters were uniformly attached to the outside of the inner tube. The results showed that the use of longitudinal fins can shorten the melting and solidification time compared to the use of the elliptical tube. Agyenim et al. [14] experimentally compared the melting and solidification performances of a shell-and-tube LHTES unit enhanced by longitudinal and transversal fins. Eight longitudinal rectangular fins with fixed structural parameters were evenly fixed outside the inner tube. The results indicated that the use of longitudinal fins can achieve a faster melting and solidification rate than the use of transversal fins. Li et al. [15] numerically studied the melting and solidification performances of a horizontal shell-and-tube LHTES unit enhanced by longitudinal fins. Six rectangular fins were evenly fixed outside the inner tube. The results indicated that the total melting/solidification time can be shortened by more than 14%. Rozenfeld et al. [16] experimentally investigated the close-contact melting in a horizontal shell-and-tube LHTES unit enhanced by longitudinal fins. Three full-length rectangular fins were evenly fixed outside the inner tube. The results indicated that close-contact melting shortens the melting time by 2.5 times.

The parameter analysis on the added fins is also a research topic in the first stage. Padmanabhan et al. [17] numerically investigated the melting and solidification characteristics of the PCM filled in a double-tube LHTES unit with evenly arranged longitudinal fins. Conduction was considered to be the only mode of heat transfer. In other words, natural convection was ignored. The results indicated that the melting/solidification rate is a function of the number of fins, fin width, and fin length. Ismail et al. [18] studied the solidification of the PCM around a vertical axially finned isothermal cylinder through numerical and experimental methods. The results showed that the number of fins and fin length have greater influence on the solidification rate of the PCM than fin width. Zhang et al. [19] numerically studied the solidification behaviors of a horizontal shell-tube LHTES unit with several longitudinal fins evenly fixed on the inner tube. The Taguchi method was utilized to optimize the fin geometry. The results suggested that the number and length of fins should be increased to obtain the best solidification behavior. Hosseini et al. [20] studied the melting behaviors of a horizontal double-tube LHTES unit with eight longitudinal fins evenly fixed on the inner tube through experimental and numerical methods. The results indicated that there is an optimal value for the fin length if the melting rate, storage capacity, and cost are considered comprehensively. Solomon et al. [21] experimentally studied the solidification behaviors of a vertical shell-tube LHTES unit with eight longitudinal fins evenly fixed on the inner tube. The results showed that setting the fin length to 60% of the annular gap is sufficient to achieve the maximum heat-transfer enhancement. Yuan et al. [22] numerically investigated the effect of the installation angle of longitudinal fins on the melting characteristics of a horizontal double-tube LHTES unit. Two longitudinal fins were evenly fixed on the outside of the inner tube. The results showed that installing one fin directly below the inner tube and another fin directly above the inner tube leads to the maximum melting rate.

Some other studies in the first stage focus on revealing the different effects of longitudinal fins on the melting and solidification processes. Abhat et al. [23] experimentally studied the melting and solidification behaviors of a horizontal double-tube LHTES unit with twelve longitudinal fins evenly fixed on the inner tube. The results showed that even if

the annular space is separated into 12 small pieces, the uneven melting phenomenon is still obvious. On the contrary, the solidification of the PCM is more uniform. This conclusion can confirm that the effect of natural convection on the melting process is more significant than on the solidification process. Bathelt et al. [24] experimentally investigated the melting and solidification around a horizontal tube. Three longitudinal fins were evenly fixed on the outside of tube. The results showed that the orientation of fins has more influence on the melting process than on the solidification process. Sparrow et al. [25] experimentally investigated the freezing around a vertical tube. Four longitudinal fins were evenly fixed on the outside of the tube. It was found that the liquid–solid interface when conduction is dominant is different from the liquid–solid interface when natural convection is dominant. Rathod et al. [26] experimentally investigated the thermal performance enhancement of a vertical shell-and-tube LHTES unit with longitudinal rectangular fins. Three fins with the same fixed structural parameters were evenly arranged. The results indicated that using fins can shorten the total melting time and solidification time by 25 and 44%, respectively. The inconsistent effects of fins on the melting and solidification process are due to the different heat-transfer mechanisms.

Natural convection leads to non-uniform melting and solidification, so recently some researchers have claimed that the fins should be arranged unevenly in order to take advantage of convection, which marks the beginning of the second stage. Since convection has more significant influence on the melting process than solidification, most of the research in the second stage focused on the melting process [27]. Wang et al. [28] numerically investigated the melting performance of a horizontal shell-and-tube LHTES unit with longitudinal rectangular fins. Three equidistant fins with the same structural parameters were placed in the bottom of the annular region. The results indicated that there is an optimal angle between adjacent fins to reduce the total melting time. Mahood et al. [29] numerically investigated the effect of fin design on the melting of the PCM in a horizontal shell-and-tube LHTES unit. Five equidistant fins with the same structural parameters were designed. The results showed that the small angle between adjacent fins and the placement of the fins in the bottom of the annular region can optimize thermal performance. Tao et al. [30] numerically investigated the effect of the number of longitudinal fins on the melting performance of a horizontal LHTES unit. Three, five, and seven equidistant fins with the same structural parameters were designed, and all the fins were placed in the bottom of the annular region. The results indicated that the local enhanced fin tube can improve the uniformity of the PCM melting process. Deng et al. [31] numerically investigated the melting performance of a horizontal shell-and-tube LHTES unit with two longitudinal rectangular fins. The effects of the location of fins and the angle between adjacent fins on the melting characteristics of the PCM were studied. The results showed that both fins should be placed in the bottom of annular region, and the best angle between the two fins should be  $120^\circ$ . Deng et al. [32] further numerically investigated the effect of the number of fins on the optimal layout of fins. The results showed that when the number of fins is less than six, all the fins should be placed in the bottom of the annular region; otherwise, the fins should be fixed evenly on the outside of the inner tube. Kumar et al. [33] investigated the effect of longitudinal finned tube eccentric configuration on melting behavior. They proposed a special arrangement of three fins to accommodate the eccentric structure. One long fin is arranged in the top region, and two short fins are arranged symmetrically in the bottom. The optimal angle between the two bottom fins was found to be  $60^\circ$ . Yagci et al. [34] studied the melting (charge) characteristics of a phase change material (PCM) in a vertical shell-and-tube LHTES unit. Four equidistant fins with the same structural parameters were fixed on the inner tube. Since the natural convection in the top is stronger than in the bottom, the fins were designed to be wedge-shaped. That is, the bottom of the fin is longer than the top. It was found that decreasing the fin edge lengths' ratio could significantly shorten the melting time, but no optimal value was proposed.

To sum up, many research studies have focused on the structural parameters optimization of longitudinal rectangular fins used in shell-and-tube LHTES unit. In addition,

many research studies focus on optimizing the structures of other types of fins [35–37]. However, most of the research is based on univariate analysis. Actually, univariate analysis is not suitable for the optimization of fin structure, because the number of structural parameters of a single fin exceeds two especially when natural convection is considered. Not to mention, the number of structural parameters will increase with the increase of the number of fins. It has been preliminary found that, to utilize the convection, the fins should not only be arranged unevenly, but also have different structural parameters. So far, few research studies have proposed fins with different structural parameters due to the expensive computational cost of phase-change optimization problems and lack of a smarter optimization method for the complex dynamic nonlinear characteristic [38]. Therefore, in this study, a modified genetic algorithm coupled with computational fluid dynamics (CFD) was developed to optimize the structural parameters of longitudinal rectangular fins in a shell-and-tube LHTES unit. The influence of natural convection on the optimal structure of fins was considered. The length, width, and position of each fin were selected as variables, and the filling rate of the fins was taken as the constraint. In this paper, the effects of the thermal conductivity of fins, the filling rate of fins, and the number of fins on the optimal structure of fins are discussed. The optimization method proposed by this paper can be used to optimize the structure of other types of fins.

## 2. Presentation of the Optimization Problem

### 2.1. Physical Model

This paper focuses on optimizing the design parameters of the longitudinal rectangular fins inserted in a horizontal single-pass shell-and-tube LHTES unit so as to accelerate the melting rate of the PCM. As shown in Figure 1, the PCM is encapsulated within the annular space between the inner and outer tube. The radii of outer and inner tube are denoted by  $r_o$  and  $r_i$ , respectively. Heat-transfer fluid (HTF) with a temperature higher than the melting point of the PCM flows in the inner tube. Heat is transferred to the PCM region through the wall of the inner tube. Several longitudinal rectangular fins are fixed on the outer surface of the inner tube to enhance heat transfer. The design parameters of fins are selected as the optimization variables, including fin length,  $l$ ; fin thickness,  $w$ ; and fin position (represented by angle  $\theta$ ). The definitions of  $l$ ,  $w$ , and  $\theta$  refer to Figure 1.

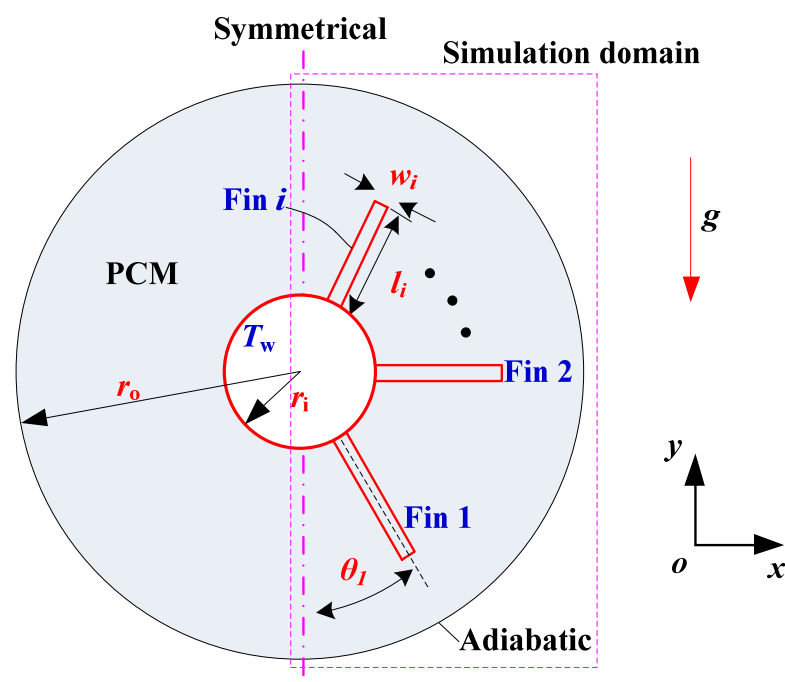


Figure 1. Physical model for present problem.

For the convenience of optimization,  $l$ ,  $w$ , and  $\theta$  are replaced by three dimensionless parameters,  $L$ ,  $\Delta$  and  $\psi$ , respectively. The definitions of these three dimensionless parameters are expressed in Equation (1). During the optimization, the three dimensionless parameters all range from 0 to 1.

$$L = \frac{l}{r_o - r_i} \quad \Delta = \frac{w}{2r_i} \quad \psi = \frac{\theta}{\pi} \quad (1)$$

The melting performance of the whole fin-enhanced LHTES unit is evaluated through studying the typical cross-section of the LHTES unit. In addition, due to the symmetry, half of the cross-section is selected as the simulation domain (see Figure 1). The wall of the inner tube is usually made of metal alloy material with high thermal conductivity, and it is far thinner than the simulation domain size, so the thickness of the wall can be ignored without having effects on the simulation results [8,39–44]. The inner tube maintains a constant temperature of  $T_w$ , and the outer tube is insulated from the environment [44]. Paraffin is selected as the PCM, and its thermo-physical properties can be found in Table 1. The values of  $T_w$ ,  $r_o$ , and  $r_i$  are 420 K, 20 mm, and 10 mm, respectively. The thermo-physical properties of the fin satisfy that the density ratio of the fin to the PCM is equal to 10.95 ( $\rho_{\text{fin}}/\rho_{\text{PCM}} = 10.95$ ), the specific heat ratio of the fin to the PCM equals 0.15 ( $c_{p,\text{fin}}/c_{p,\text{PCM}} = 0.15$ ), and the thermal conductivity ratio of the fin to the PCM varies from 83.6 to 1987.7 ( $\lambda_{\text{fin}}/\lambda_{\text{PCM}} = 83.6 - 1987.7$ ).

**Table 1.** Physical properties of paraffin [45].

Physical Properties	Paraffin
$\rho$ ( $\text{kg m}^{-3}$ )	820
$c_p$ ( $\text{J kg}^{-1} \text{K}^{-1}$ )	2500
$\lambda$ ( $\text{W m}^{-1} \text{K}^{-1}$ )	0.195
$\mu$ ( $\text{kg s m}^{-1}$ )	0.205
$\gamma$ ( $\text{K}^{-1}$ )	0.0006
$L$ ( $\text{J kg}^{-1}$ )	210,000
$T_{m1}$ (K)	320.66
$T_{m2}$ (K)	321.66

## 2.2. Governing Equations

Numerical methods are employed to solve the optimization problem of the fin structure. In the traditional numerical simulation process, the parameters of the fins need to be determined first. The grids of the fin area and the phase-change material area are drawn according to these parameters. Each specific parameter corresponds to a specific group of grids. However, in the optimization process, the parameters of the fins are unknown and obtained through the optimization process. If the traditional method is used, a large number of grids need to be drawn, and this is time-consuming. Therefore, in order to improve the computing efficiency, the unified governing equations are used in this study to describe the phase-change heat transfer of the PCM and the pure heat conduction of the fins. The enthalpy–porosity model is employed to express the solid–liquid phase change process, and the porous model is used to differentiate the fin region from the PCM region. The governing equations, namely the energy equation, continuity equation, and momentum equation, are listed as follows.

Energy equation [42]:

$$\begin{aligned} & [(1 - \varepsilon)(\rho c_p)_{\text{fin}} + \varepsilon(\rho c_p)_{\text{PCM}}] \frac{\partial T}{\partial t} + \varepsilon \rho_{\text{PCM}} \Delta h \frac{\partial f}{\partial t} + (\rho c_p)_{\text{PCM}} \left( u \frac{\partial T}{\partial x} + v \frac{\partial T}{\partial y} \right) \\ & = [\varepsilon \lambda_{\text{PCM}} + (1 - \varepsilon) \lambda_{\text{fin}}] \left( \frac{\partial^2 T}{\partial x^2} + \frac{\partial^2 T}{\partial y^2} \right) \end{aligned} \quad (2)$$

where  $\varepsilon$  is an integer used to distinguish the fin region from the PCM region. For the fin region and the PCM region,  $\varepsilon$  is equal to 0 and 1, respectively; and  $f$  in the second term on

the left side of Equation (2) is the liquid fraction of the PCM, whose definition is given in Equation (3). Solidification temperature,  $T_s$ , is 1 K lower than the melting temperature,  $T_m$ .

$$\begin{cases} f = 1 & T > T_m \\ f = \frac{T-T_s}{T_m-T_s} & T_s < T < T_m \\ f = 0 & T < T_s \end{cases} \quad (3)$$

Momentum equations [41]:

*x*-direction:

$$\rho \left( \frac{\partial u}{\partial t} + u \frac{\partial u}{\partial x} + v \frac{\partial u}{\partial y} \right) = \mu \left( \frac{\partial^2 u}{\partial x^2} + \frac{\partial^2 u}{\partial y^2} \right) - \frac{\partial p}{\partial x} - \frac{\mu}{K} u - A_{\text{mush}} \frac{(1-f)^2}{f^3 + \delta} u \quad (4)$$

*y*-direction:

$$\begin{aligned} \rho \left( \frac{\partial v}{\partial t} + u \frac{\partial v}{\partial x} + v \frac{\partial v}{\partial y} \right) &= \mu \left( \frac{\partial^2 v}{\partial x^2} + \frac{\partial^2 v}{\partial y^2} \right) - \frac{\partial p}{\partial y} - \frac{\mu}{K} v - A_{\text{mush}} \frac{(1-f)^2}{f^3 + \delta} v \\ &+ \rho_{\text{ref}} g \beta (T - T_{\text{ref}}) \end{aligned} \quad (5)$$

The third terms on the right side of Equations (4) and (5) are the viscous loss terms from the porous model. In the fin region, the permeability ( $K$ ) is set to an extremely small value ( $10^{-20} \text{ m}^2$ ), which means no flow in the fin region, while in the PCM region,  $1/K$  is set to zero.  $A_{\text{mush}}$  is the mushy zone constant with a value of  $10^5 \text{ kg m}^{-3} \text{ s}^{-1}$  [40], and  $\delta$  is a small constant (0.001) to prevent the denominator from being equal to zero. The fifth term on the right side of Equation (5) is used to estimate the effect of natural convection on the velocity field.

Continuity equation:

$$\frac{\partial u}{\partial x} + \frac{\partial v}{\partial y} = 0 \quad (6)$$

### 2.3. Numerical Method

The governing Equations (2)–(6) are solved numerically through the FVM (finite volume method) because they have no analytical solutions. The unified governing equations make it feasible to construct fins with different structural parameters in a fixed grid system, and the detailed method can be found in our previous articles [42,43,46–49]. For specific settings of the FVM, see Ref. [50].

To determine the appropriate mesh size, a single-fin case is studied. As shown in Figure 2, the dimensionless length,  $L$ ; thickness,  $\Delta$ ; and angle,  $\psi$ , of the fin are set to 0.5, 0.05, and 0.5, respectively. The thermal conductivity ratio of the fin to the PCM (denoted as  $\lambda_{\text{fin}}/\lambda_{\text{PCM}}$ ) is set to 1987.7. Four grid sizes are designed, and the total number of grids in the whole simulation domain is 819, 2765, 12,346, and 48,269, respectively. In addition, the cases with different grid numbers have different time steps so as to determine the appropriate time step. Figure 2 shows the variation of dimensionless total melting time,  $Fo_{\text{tot}}$ , with the number of grids. The dimensionless melting time is expressed by the Fourier number,  $Fo$ , and its definition is given in Equation (7).  $Fo_{\text{tot}}$  can be calculated by substituting the total melting time,  $t_{\text{tot}}$ , for  $t$  in Equation (7). It can be seen from Figure 2 that, for the grid numbers 48,269 and 12,346, the deviation of  $Fo_{\text{tot}}$  is only 0.02%.

Fourier number:

$$Fo = \frac{t\alpha}{D_e^2}, D_e = D_o - D_i \quad (7)$$

Figure 3 shows the effect of the number of grids on the distribution of dimensionless thermal conductivity. The dimensionless thermal conductivity is defined as the thermal conductivity ratio of the local grid to the PCM. The outline of the fin can be seen from the distribution graph of the dimensionless thermal conductivity. It can be seen from Figure 3

that the more grids there are, the clearer the outline of the fin. The fin structure is very close to the real one when the number of grids is 48,269. The comparison results shown in Figures 2 and 3 can prove that the fourth grid system with a grid number of 48,269 and a time step of 0.1 s is suitable for studying the optimization problem presented in this paper.

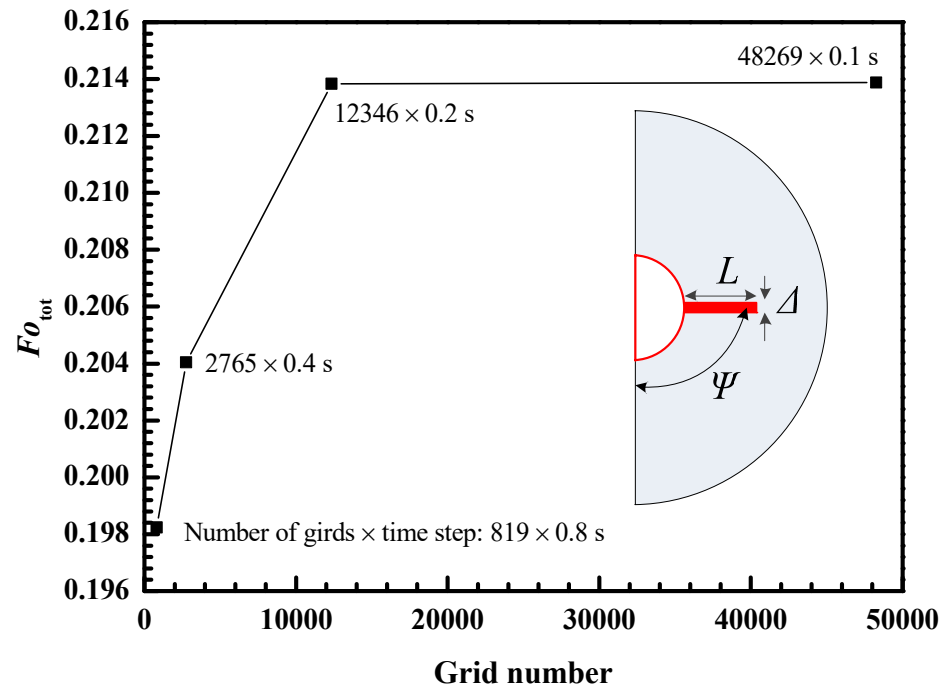


Figure 2. Variation of dimensionless total melting time with grid number.

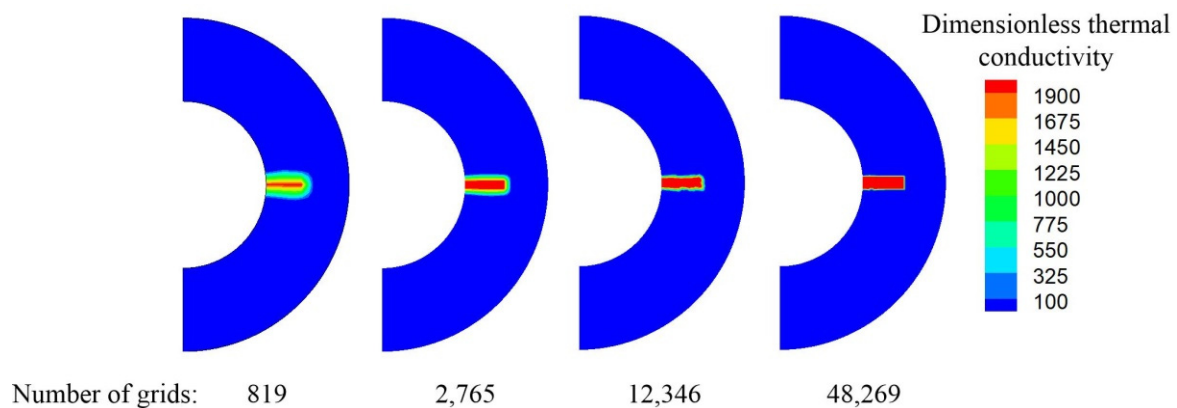


Figure 3. Effect of the number of grids on the distribution of dimensionless thermal conductivity.

The mathematical model presented in Section 2.3 has been widely used to investigate the solid–liquid phase-change problem. Our previous articles have verified the accuracy of this model through comparing the numerical results with the experimental data and analytical solutions. The verification of the model can be found in Refs. [40–43,50] and is not repeated here.

#### 2.4. Optimization Method

The optimization problem that concerns this paper is listed in Table 2. The design parameters of the fins under different numbers and total areas of fins ( $L_i$ ,  $\Delta_i$ ,  $\theta_i$ ) are selected as variables. The total melting time,  $t_{tot}$ , is taken as the optimization objective. The number of variables depends on the number of fins. For example, there are two variables for one fin and five variables for two fins.

**Table 2.** Description of the optimization problem.

Optimization function:	$\text{Min}(t_{\text{tot}}) = \text{Fun}\{L_i, \Delta_i, \theta_i\}$
Constraint:	The dimensionless fin area ( $A$ ) is fixed

The genetic algorithm (GA) was chosen as the optimization method because it is suitable for solving nonlinear optimization problems [51]. Due to the expensive computational cost of phase-change optimization problems, a new coupling algorithm between GA and CFD is proposed. The flowchart of this new coupling algorithm is shown in Figure 4. The characteristics of this new coupling algorithm are summarized as follows.

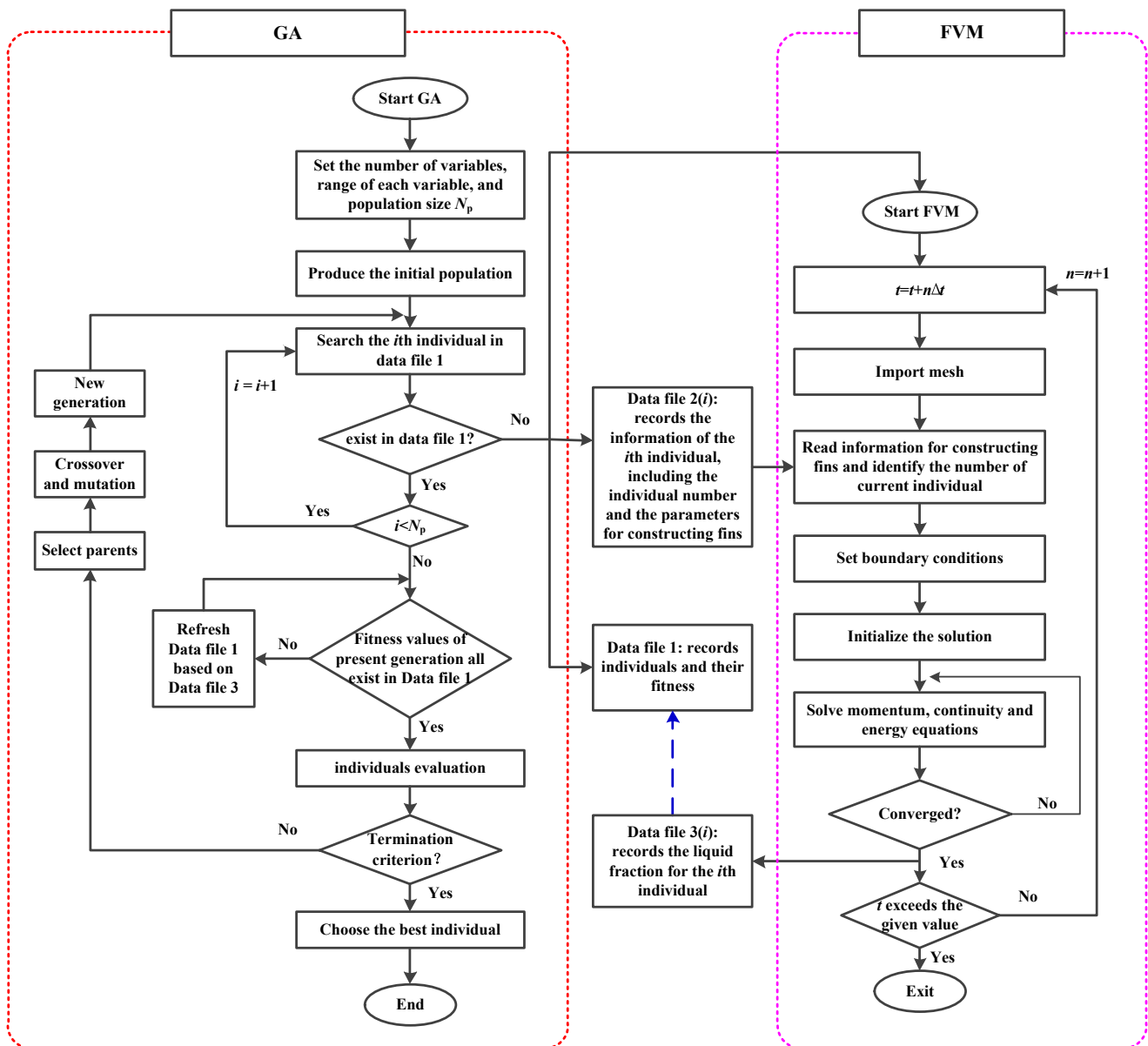


**Figure 4.** The flowchart of the optimization process.

The first characteristic is that Data File 1 is used to record all individuals generated by GA and their fitness values. Each individual is composed of independent variables with fixed values, and the number of variables of each individual is equal to the number of variables of the optimization problem. Data File 1 is used for two reasons: one reason is that some excellent individuals with low fitness values will be preserved from the present

generation to the next generation. Since the new algorithm searches Data File 1 for the fitness evaluation, Data File 1 can ensure that the GA needs to call the CFD only once for the same individual. Most of the optimization time is spent on the iterations of the CFD, so reducing the number of CFD calls can greatly reduce the time consumption. Another reason is that Data File 1 is very useful in dealing with the unexpected interruption of the optimization process caused by power failure or computer restart.

The second characteristic of the new algorithm is that the CFD can be called in parallel to estimate the fitness of all individuals in the same generation. Calling the CFD in parallel is the most effective way to reduce the time cost. Nevertheless, the next generation is allowed to be created only after the fitness assessment of all individuals in the current generation has been completed. The third characteristic of the new algorithm is that the series of data files named Data File 3 (*i*) is created to record the real-time evaluation progress of each individual. Data File 3 can be used to refresh Data File 1 and monitor the running CFD cases.

Optimization starts with GA. GA randomly creates the first generation of individuals and searches for each individual in Data File 1. If an individual does not exist, FVM will be called to calculate the fitness value of that individual. After checking all individuals, if the fitness value of some individuals has not been finished, the GA will pause. A loop is used to pause the GA and refresh the fitness value recorded in Data File 1. If the fitness calculation of the first generation is completed, the GA enters the loop of the second generation. More details on the combination between the GA and FVM can be found in Ref. [52].

### 3. Results and Discussion

The purpose of this paper is to optimize the structural parameters of fins with a given fin area and improve the melting rate of a shell-and-tube latent heat storage unit. In this section, some novel fin structures are presented, and the effects of fin thermal conductivity, fin area, and fin number on the optimization results are discussed.

#### 3.1. Optimization Results of a Single Fin in Half Ring Region

The structural parameters of a single fin with a given fin area are optimized in this section. The dimensionless fin area (the ratio of fin area to simulation-domain area) is fixed to 0.02 ( $A = 0.02$ ). The thermal conductivity ratio of the fin to the PCM is fixed at 1987.7 ( $\lambda_{\text{fin}}/\lambda_{\text{PCM}} = 1987.7$ ). In this case, an individual consists of two variables: the dimensionless fin length and fin angle ( $L$  and  $\psi$ ). The definitions of  $L$  and  $\psi$  refer to Equation (1). Both the  $L$  and  $\psi$  can vary from 0 to 1. The fin width can be calculated if  $L$  and  $\psi$  have specific values.

For genetic algorithms, the population size is a key parameter to determine the accuracy of the optimization results. Figures 5 and 6 give the fitness values of dimensionless total melting time ( $F_{0\text{tot}}$ ) for different  $L$  and  $\psi$  values generated by the genetic algorithm (GA) with different population sizes. Theoretically, the larger the population size is, the better the optimization result is, because that larger population size will lead to more individuals generated by GA. However, from the results shown in Figures 5 and 6, it is the population size of 10 rather than 20 or 40 that produces a minimum  $F_{0\text{tot}}$ . This is due to the randomness of the GA. Despite the minor difference, the optimization results for the three population sizes are consistent. As shown in Figure 6,  $F_{0\text{tot}}$  first decreases and then increases with  $\psi$ . The optimal individuals with population size of 10, 20, and 40 are named Optimal Case 1, 2, and 3, respectively. The  $L$  and  $\psi$  of the Optimal Case 1 are 0.964 and 0.199, respectively. Compared with the Optimal Cases 1, the  $L$  of the Optimal Cases 2 and 3 has only a deviation of 2% and 0.9%, and the  $\psi$  of the Optimal Cases 2 and 3 has only a deviation of 3.7% and 1.6%. From the view of the fitness value ( $F_{0\text{tot}}$ ), the deviations between Optimal Cases 1 and 2 and between Optimal Cases 1 and 3 are as low as 1.3% and 0.4%, respectively.

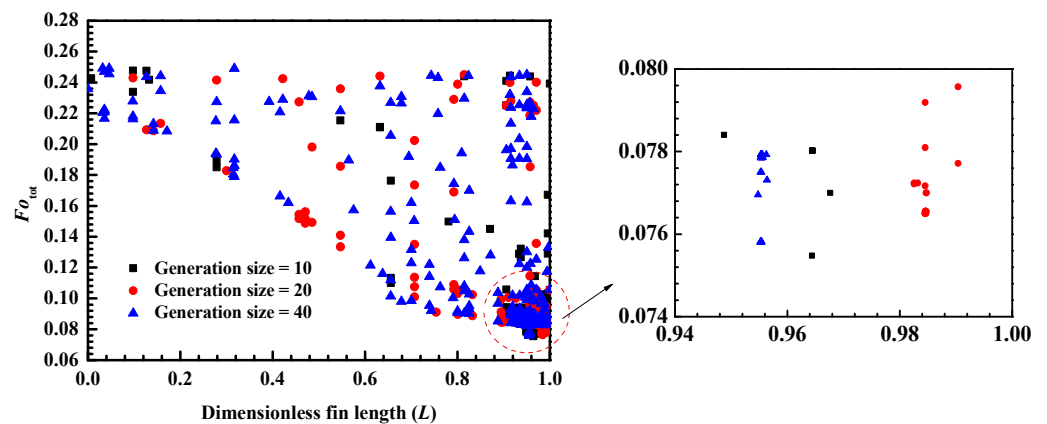


**Figure 5.** Different dimensionless fin lengths generated by genetic algorithm (GA) with different population sizes.

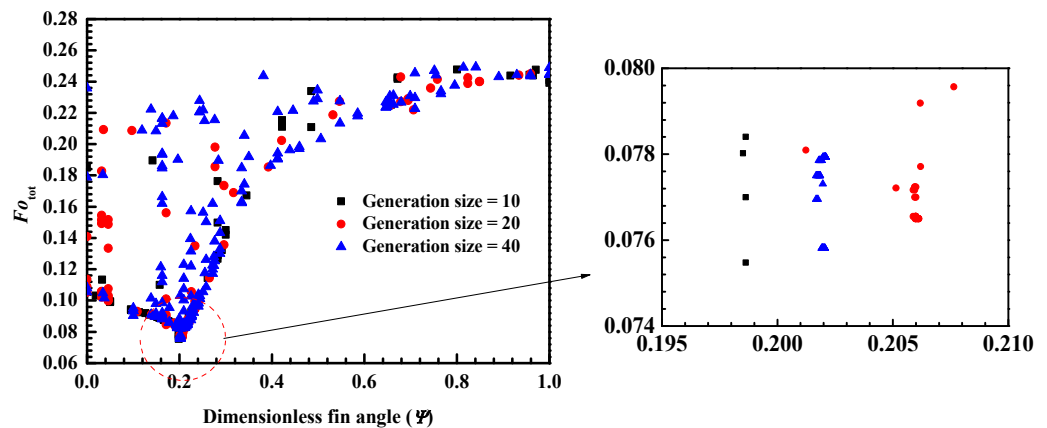


**Figure 6.** Different dimensionless fin angles generated by genetic algorithm (GA) with different population sizes.

Increasing population size will lead to a huge surge in optimization time and CPU assumption, because many more CFD cases will be awakened. When population sizes are 10, 20, and 40, the number of calls to CFD is 140, 239, and 474, respectively. To control the time cost and guarantee the accuracy, the population size of 20 is selected for all the following cases.

To reveal why using the structural parameters optimized by GA can obtain the highest melting rate, the melting characteristic of the Optimal Case 1 is compared with three special cases. Special Case 1 has no fin. In Special Case 2, a single fin is placed in the bottom of the domain. In other words, the  $L$  and  $\psi$  of Special Case 2 are 1.0 and 0, respectively. Special Case 3 has the same  $\psi$  as Optimal Case 1, but its  $L$  is 1.0.

Figure 7 shows the distribution of liquid fraction and velocity magnitude  $(u^2+v^2)^{0.5}$  for Special Cases 1–3 and Optimal Case 1 at three moments. In each annular region, the left half is the distribution of liquid fraction, and the right is the distribution of velocity magnitude. In the left half, the blue region denotes the non-melted region (solid PCM), and the red region represents the fully melted region (liquid PCM). It can be observed from the contour map of Special Case 1 that natural convection results in non-uniform melting. The melting rate of the PCM in the top region is higher than in the bottom region. Inserting the fin in the bottom, like in Special Case 2, is helpful to decrease the  $Fo_{tot}$ . However, a large area of the solid PCM can still be found in the bottom region when  $Fo = 0.071$ . This phenomenon indicates that inserting the fin vertically under the inner tube is not the best solution. The fin used in Special Case 3 is longer and thinner than that in Optimal Case 1 since the fin area is fixed. From the contour graphs of Special Case 3, it can be seen that the fin is helpful to accelerate the melting of the PCM in the lower region. There is more solid PCM in the

upper part of the fin than in the lower part when  $Fo = 0.071$ . This non-uniform melting phenomenon leads to an increase in the total melting time. On the contrary, a more uniform melting can be found in the contour graphs of Optimal Case 1. Therefore, a well-designed fin should ensure that the PCM in the different regions tends to have a consistent melting rate. Figure 8 gives the dimensionless total melting time,  $Fo_{tot}$ , for Special Cases 1–3 and Optimal Case 1. It can be seen that Optimal Case 1 has the minimum  $Fo_{tot}$ . Compared with the case of no fin (Special Case 1), The use of optimal fins can shorten the dimensionless total melting time by 68%.

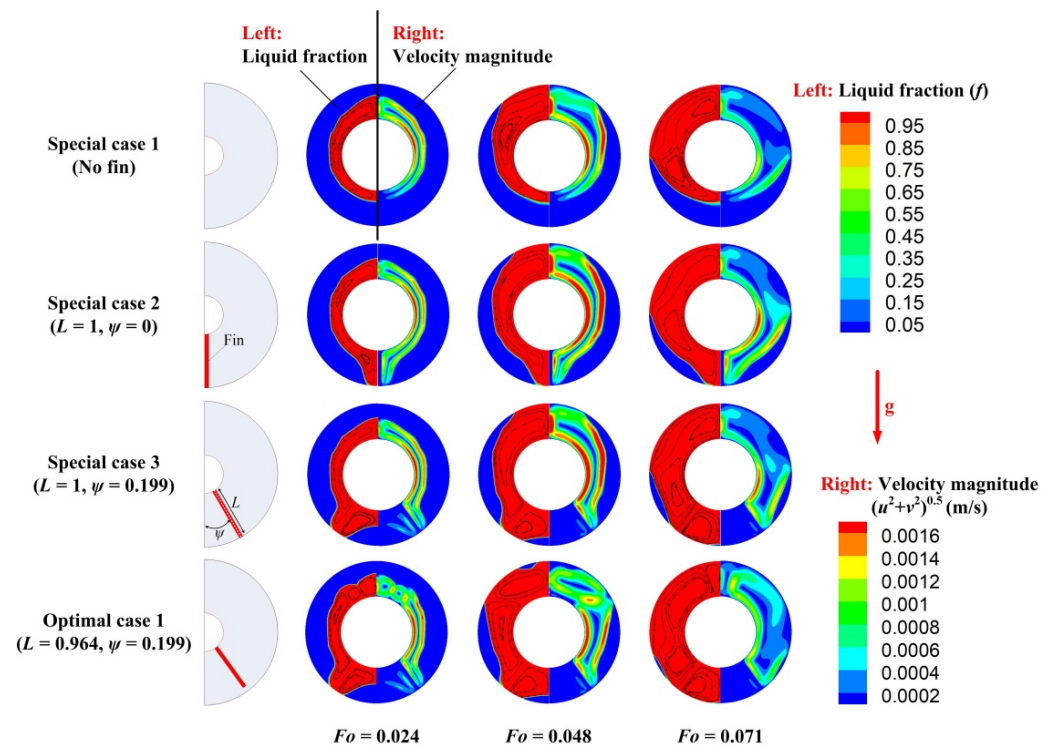


**Figure 7.** Contour maps of liquid fraction and velocity magnitude for Special Cases 1–3 and Optimal Case 1.

Based on the optimal results of GA, the optimal value of  $\psi$  is about 0.2, which means that the fin is still in the lower half of the annular region. Actually, the optimal value of  $\psi$  depends on the magnitude of convection relative to conduction. When convection plays a more significant role in heat transfer than conduction, the value of  $\psi$  should be reduced. On the contrary, if the conduction is dominant in the heat transfer, the value of  $\psi$  should be increased. For an extreme case of neglecting natural convection, the best value of  $\psi$  should be 0.5. That is, the fin should be placed in the middle region between the upper and lower parts of the annular space. Therefore, natural convection is a sensitive parameter that affects the optimal position and structure of the fin.

### 3.2. Effect of Fin Thermal Conductivity on the Optimal Structural Parameters of Fin

This section discusses the effect of the thermal conductivity ratio of the fin to the PCM (denoted as  $\lambda_{fin}/\lambda_{PCM}$ ) on the optimal structure parameters of the fin. The single fin with dimensionless area of 0.02 ( $A = 0.02$ ) is considered. Figure 9 shows the variation of the optimal structure parameters (dimensionless fin length,  $L$ , and dimensionless fin angle,  $\psi$ ) with  $\lambda_{fin}/\lambda_{PCM}$  when the population size is 20. The  $\lambda_{fin}/\lambda_{PCM}$  changes from 83.6 to 1987.7. It can be seen from Figure 9 that the optimal values of  $L$  and  $\psi$  both increase with the increase of  $\lambda_{fin}/\lambda_{PCM}$ . Increasing the  $\lambda_{fin}/\lambda_{PCM}$  leads to the increase of heat conduction through the fin. In other words, heat conduction plays a more important role in total heat transfer. Therefore, the value of  $\psi$  should be increased to move the fin from the bottom toward the middle. As for  $L$ , its value should be carefully designed to balance the melting

progress in the upper and lower regions of the fin. It also can be found from Figure 9 that, although the value of  $\lambda_{fin}/\lambda_{PCM}$  is increased by nearly 24 times, the optimal values of  $L$  and  $\psi$  are only increased by 14.7% and 11%, respectively. This is because most of the heat absorbed by the PCM is not through the fin since the fill rate of the fin is low. In addition, increasing  $\lambda_{fin}/\lambda_{PCM}$  does not significantly affect the role of natural convection in total heat transfer. Therefore,  $\lambda_{fin}/\lambda_{PCM}$  is not a sensitive parameter that affects the optimal position and structure of the fin.

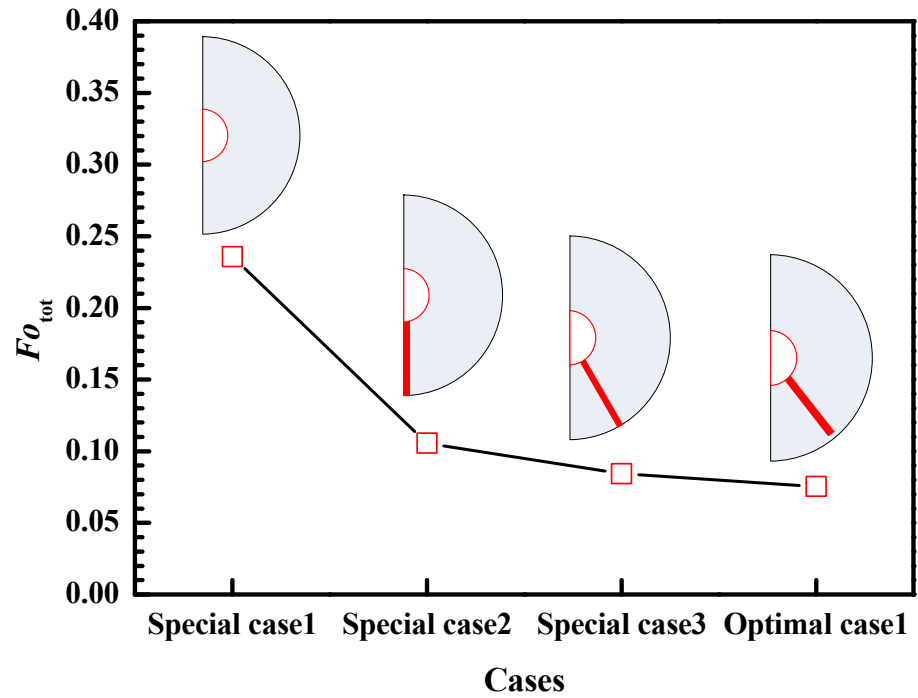


Figure 8. Dimensionless total melting time,  $Fo_{tot}$ , for Special Cases 1–3 and Optimal Case 1.

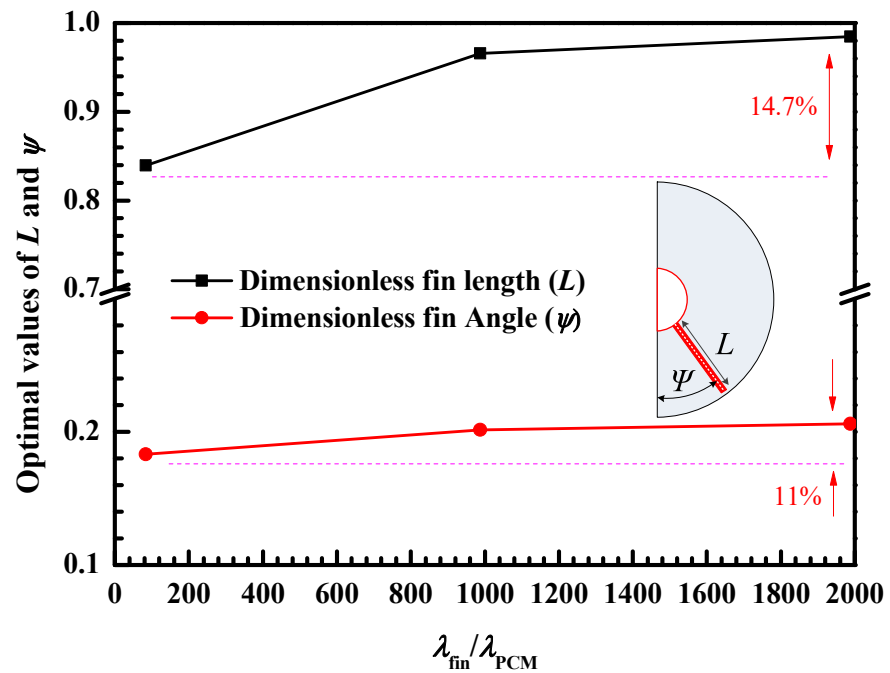


Figure 9. Variation of the optimal dimensionless fin length,  $L$ , and dimensionless fin angle,  $\psi$ , with the thermal conductivity ratio of fin to PCM ( $\lambda_{fin}/\lambda_{PCM}$ ).

Figure 10 shows the distribution of liquid fraction and dimensionless temperature for Optimal Cases 2, 4, and 5 at three moments. Optimal Case 2 is mentioned in Section 3.1, which uses the fin optimized for  $\lambda_{fin}/\lambda_{PCM} = 1987.7$ . Optimal Cases 4 and 5 use the fins optimized for  $\lambda_{fin}/\lambda_{PCM} = 1037.9$  and  $\lambda_{fin}/\lambda_{PCM} = 83.6$ , respectively. It can be seen from Figure 10 that the melting progress of these three optimal cases is almost the same.

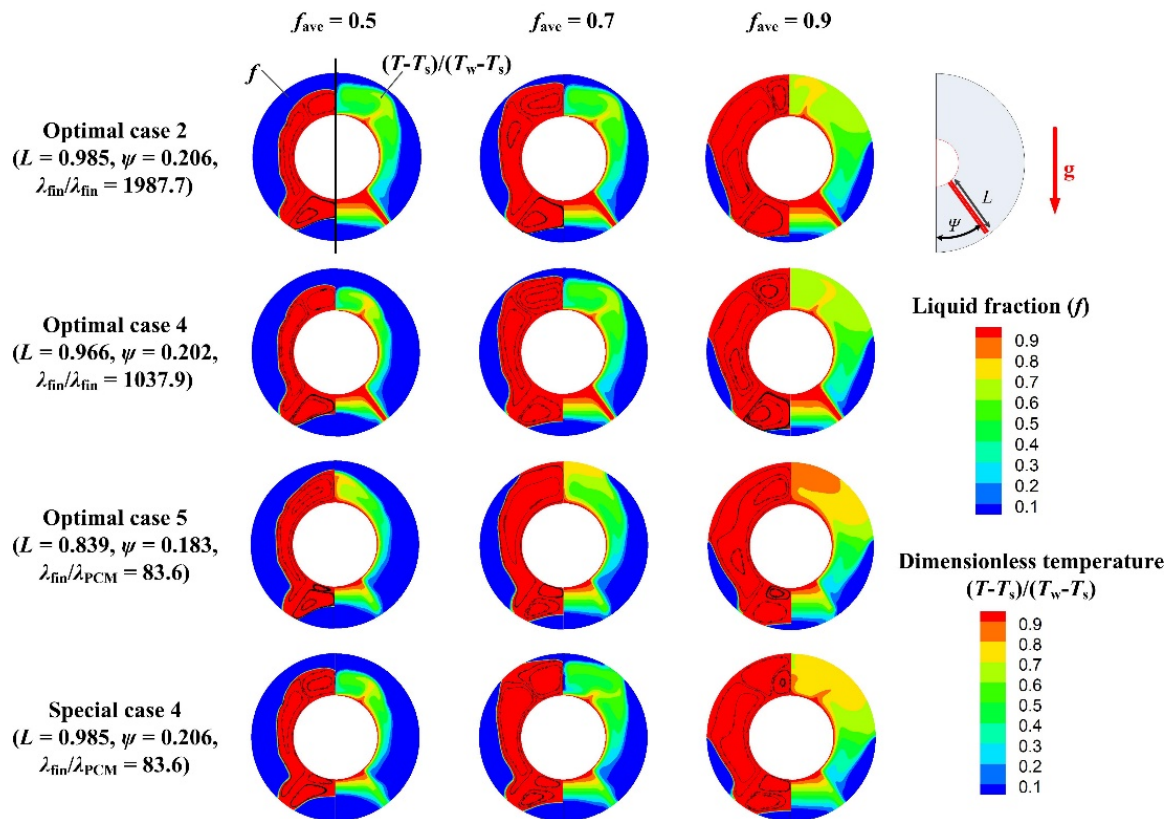


Figure 10. Contour maps of liquid fraction and dimensionless temperature for Optimal Cases 2, 4 and 5 and Special Case 4.

To further prove different fin designs for different  $\lambda_{fin}/\lambda_{PCM}$  values, a special case called Special Case 4 was designed. Special Case 4 uses the same fin as Optimal Case 2, but the  $\lambda_{fin}/\lambda_{PCM}$  is set to 83.6. The distribution of liquid fraction and dimensionless temperature for Special Case 4 is also shown in Figure 10. It can be seen that, for the same  $\lambda_{fin}/\lambda_{PCM}$ , the melting rate of the PCM under the fin in Special Case 4 is slower than that in Optimal Case 5. Figure 11 gives the variation of the liquid fraction ( $f$ ) with the dimensionless melting time ( $Fo$ ) for Optimal Case 5 and Special Case 4. It can be seen that Optimal Case 5 has a faster later-stage melting rate than Special Case 4. When  $Fo = 0.095$ , the PCM in Optimal Case 5 has been completely melted ( $f = 1.0$ ), while the solid PCM can still be found in the bottom of the annular region in Special Case 4.

### 3.3. Effect of Fin Area on the Optimal Structural Parameters of Fin

In this section, the effect of fin area on the optimal structure parameters of fin is studied. The dimensionless fin area,  $A$ , varies from 0.02 to 0.1, and the number of fins is fixed at 1. The definition of  $A$  refers to Section 3.1. The thermal conductivity ratio of the fin to the PCM is fixed at 1987.7 ( $\lambda_{fin}/\lambda_{PCM} = 1987.7$ ). Figure 12 shows the variation of the optimal dimensionless fin length ( $L$ ) and dimensionless fin angle ( $\psi$ ) with  $A$  when the population size is 20. It can be seen that  $\psi$  increases with the increase of  $A$ . The reason is that the role of heat conduction in total heat transfer becomes more important with the increase of  $A$ . Although increasing  $\lambda_{fin}/\lambda_{PCM}$  and fin area both increase the role of heat conduction, they have different effects on the optimal  $L$ . It can be found from Figures 9 and 12 that the

optimal  $L$  increases with the increase of  $\lambda_{fin}/\lambda_{PCM}$ , while it decreases with the increase of the fin area. This result indicates that, unlike the optimal  $\psi$ , the optimal  $L$  does not simply change with the relative size of heat conduction and natural convection.

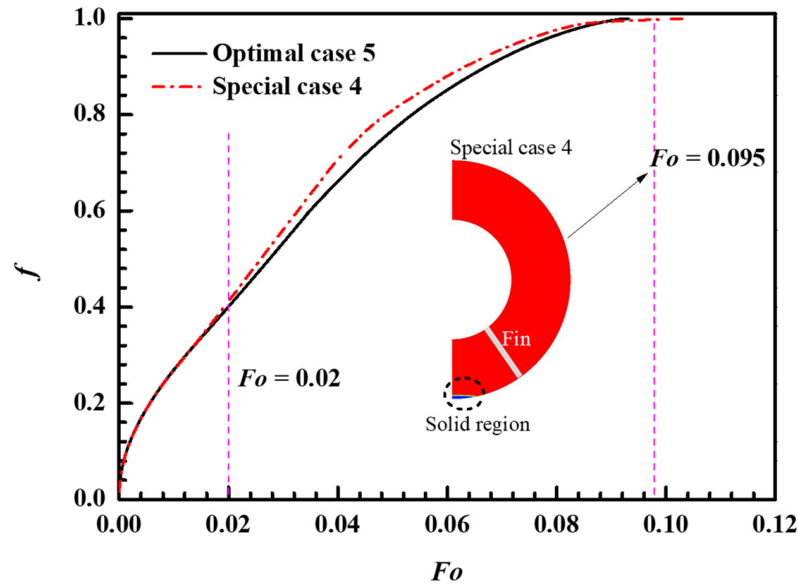


Figure 11. Variation of the liquid fraction,  $f$ , with dimensionless melting time,  $Fo$ , for Optimal Case 5 and Special Case 4.

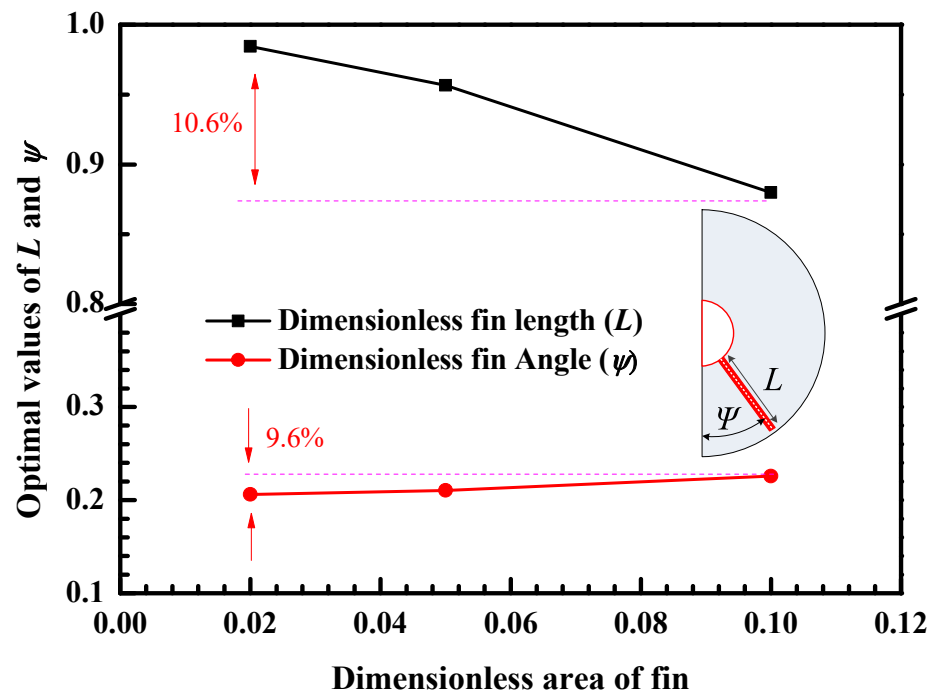
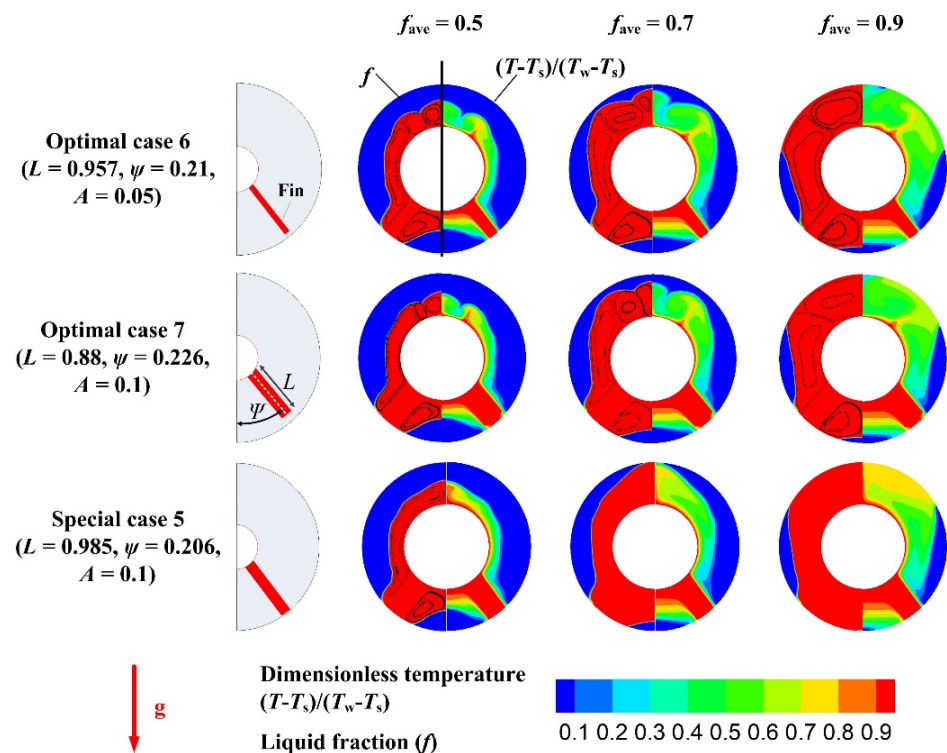


Figure 12. Variation of the optimal dimensionless fin length,  $L$ , and dimensionless fin angle,  $\psi$ , with the dimensionless fin area,  $A$ .

Figure 13 shows the distribution of liquid fraction and dimensionless temperature for Optimal Cases 6 and 7 at three moments. Optimal Cases 6 and 7 use the fins optimized for  $A = 0.05$  and  $A = 0.1$ , respectively. For the optimal design of fin for  $A = 0.02$ , see Optimal Case 2 mentioned in Section 3.1. The contour maps of Optimal Case 2 can be found in Figure 10, so it is not repeated in Figure 13. It can be seen that these three optimal cases

have almost the same melting process, and the PCM in the upper and lower region of the fin has a similar melting ratio.



**Figure 13.** Contour maps of liquid fraction and dimensionless temperature for Optimal Cases 6 and 7 and Special Case 5.

It also can be found from Figure 12 that although the value of  $A$  is increased by four times, the optimal values of  $L$  and  $\psi$  only change by 10.6% and 9.6%, respectively. It means that the fin area or fin fill rate is not a sensitive parameter for the optimal position and structure of the fin. In fact, in order to maintain the heat storage capacity, reduce the investment cost, and control the total mass of the device, the fin area is not allowed to increase excessively.

To further prove that there should be different fin designs for different  $A$  values, a special case called Special Case 5 was designed. The values of  $L$  and  $\psi$  of Special Case 5 are the same as Optimal Case 2, but the  $A$  of Special Case 5 is set to 0.1. That is to say, the fin used in Special Case 5 is thicker than the fin used in Optimal Case 2. The distribution of liquid fraction and dimensionless temperature for Special Cases 5 is also shown in Figure 13. It can be observed that, compared with the fin design of Optimal Case 7, the fin design of Special Case 5 results in a greater melting rate of the PCM under the fin. Figure 14 gives the variation of the liquid fraction,  $f$ , with the dimensionless melting time,  $Fo$ , for Optimal Case 7 and Special Case 5. It can be seen that when the dimensionless melting time exceeds 0.02 ( $Fo > 0.02$ ), Optimal Case 7 has a faster melting rate than Special Case 5. When  $Fo = 0.076$ , the PCM in Optimal Case 7 has been completely melted ( $f = 1.0$ ), while the solid PCM can still be found in the upper region of Special Case 5. From Figures 13 and 14, it can be concluded that the optimal fin can make the melting more uniform, thus shortening the melting time.

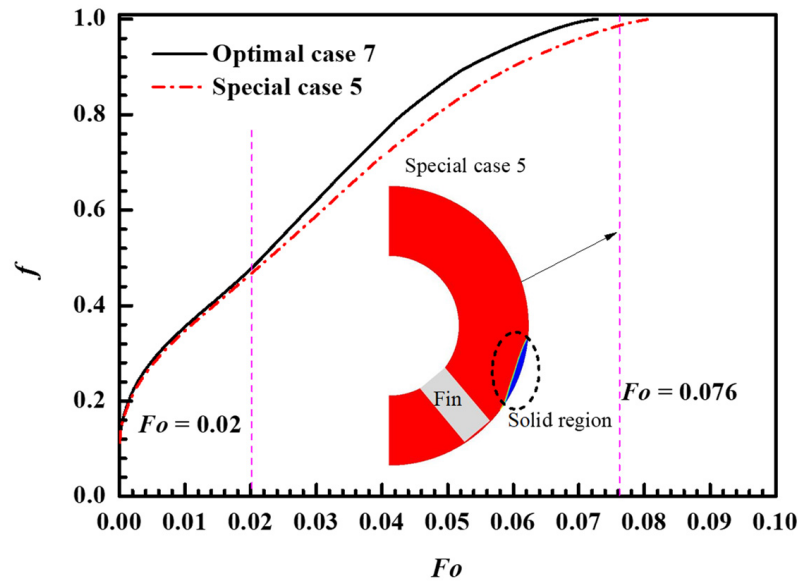


**Figure 14.** Variation of liquid fraction,  $f$ , with the dimensionless melting time,  $Fo$ , for Optimal Case 7 and Special Case 5.

**3.4. Effect of the Number of Fins on the Optimal Structural Parameters of Fins**

In this section, the effect of the number of fins on the optimization results is discussed. The dimensionless fin area is fixed at 0.05, and the thermal conductivity ratio of the fin to the PCM is 1987.7 ( $\lambda_{fin}/\lambda_{PCM} = 1987.7$ ). The structure and position of single fin, double fins, and four fins are optimized. For the structure and position of the single fin, see Optimal Case 2, which is given in Figure 10. The optimal structure and position of the double fins and four fins are given in Figure 15. It can be seen that if the number of fins is one or two, all fins should be placed in the lower half, indicating that natural convection is still dominant. However, when the number of fins reaches four, the fins are arranged almost uniformly. This signifies that conduction is dominant. Figure 16 gives the contour maps of liquid fraction and velocity magnitude for Optimal Cases 8 and 9. Optimal Cases 8 and 9 use the optimized two fins and four fins, respectively. It can be seen that the velocity magnitude  $(u^2+v^2)^{0.5}$  of Optimal Case 9 is obviously slighter than that of Optimal Case 8 when  $Fo = 0.36$ . This result means that, in Optimal Case 9, which has four fins, natural convection is relatively weak, so the effects of heat conduction play a bigger role.

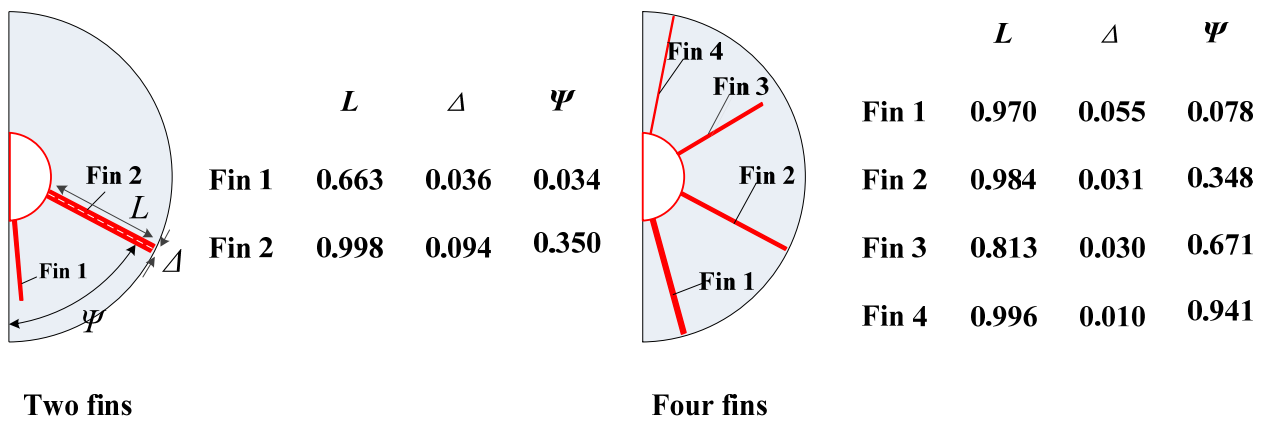


**Figure 15.** Optimal structure and position of the double fins and four fins.

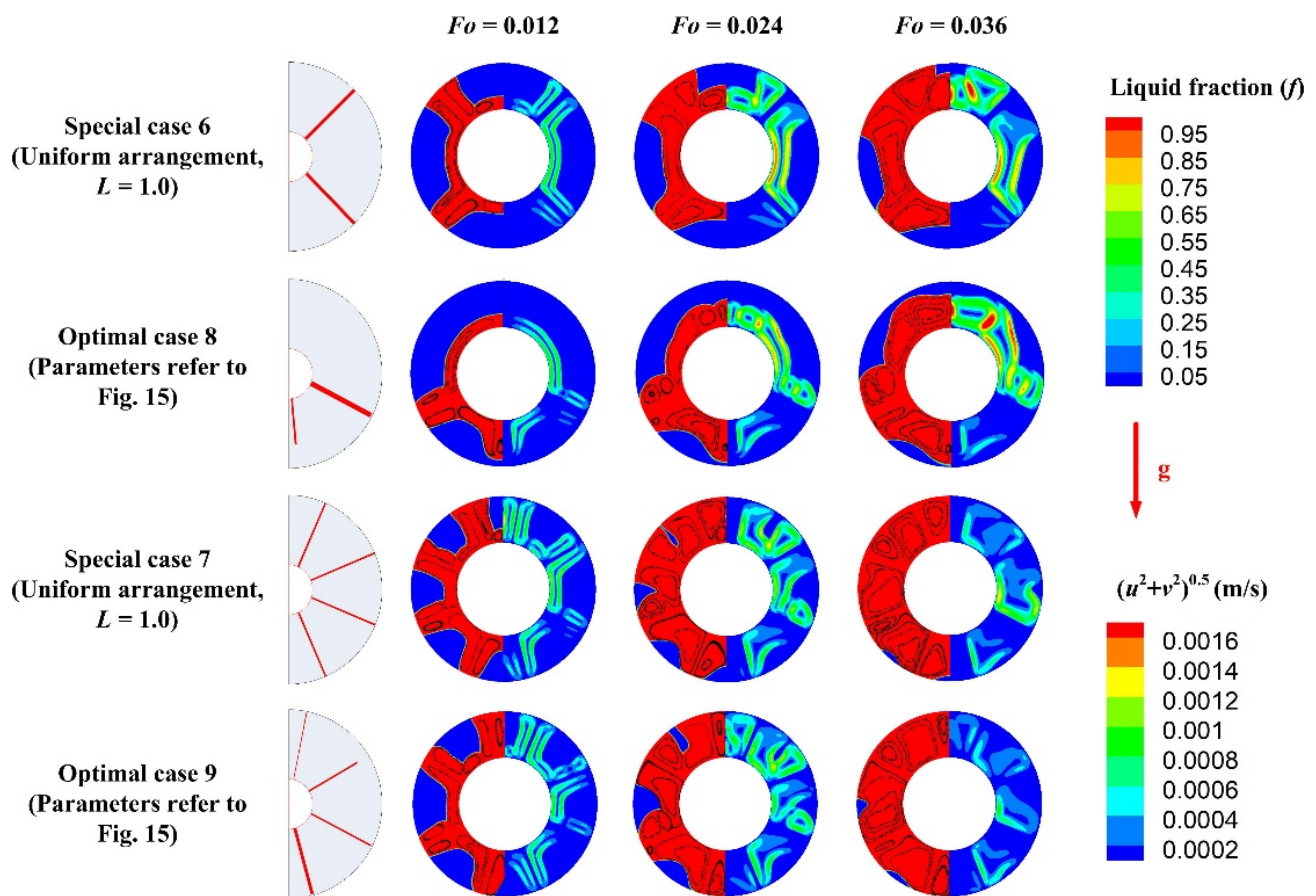


**Figure 16.** Contour maps of liquid fraction and velocity magnitude for Special Cases 6 and 7 and Optimal Cases 8 and 9.

Figure 15 also shows that when the number of fins exceeds one, different fins have different structures and locations after the optimization. To prove this, two special cases named Special Cases 6 and 7 were designed. Case 6 has two fins, and Case 7 has four fins. All the fins in Special Cases 6 and 7 have a full length ( $L = 1.0$ ) and are uniformly arranged. The contour maps of liquid fraction and velocity magnitude for Special Cases 6 and 7 are also given in Figure 16. It can be seen that, compared with the optimized fins, the uniformly arranged fins lead to a more solid PCM in the bottom region. This limits the later melting rate because the PCM in the bottom is difficult to melt. Figure 17 shows the comparison of dimensionless total melting time,  $Fo_{tot}$ , with optimized fins and uniformly arranged fins. It can be seen that using optimized fins can obtain a smaller  $Fo_{tot}$  compared with using uniformly arranged fins. The highest reduction of  $Fo_{tot}$  is 61.3% when one fin is used. As the number of fins increases, the reduction of  $Fo_{tot}$  decreases. This is because, as the number of fins increases, the role of conduction in total heat transfer becomes more important. When the number of fins is four,  $Fo_{tot}$  can still be reduced by 15.9%, which indicates that natural convection still has a significant effect on heat transfer. The results of this section indicate that the number of fins is a sensitive parameter that affects the optimal position and structure of the fins.

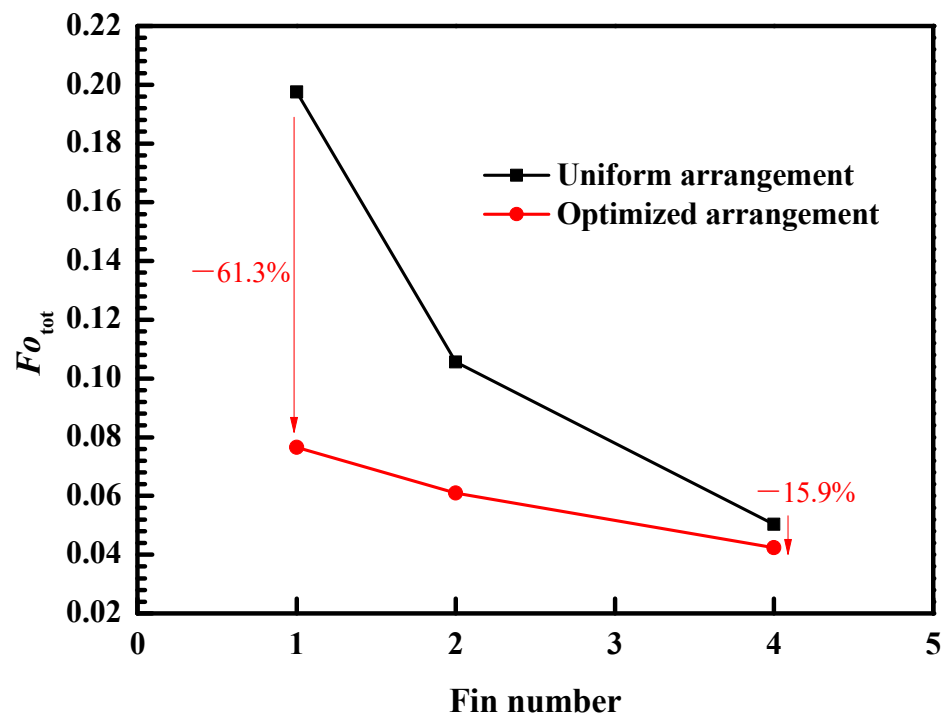


Figure 17. Variation of dimensionless total melting time,  $Fo_{tot}$ , with the number of fins.

#### 4. Conclusions

Longitudinal rectangular fins are commonly applied in the shell-and-tube latent heat storage unit for melting-performance enhancement. In this study, a new coupling algorithm between genetic algorithm (GA) and computational fluid dynamics (CFD) was developed to optimize the structural parameters of the fins. The total melting time is selected as the objective; the length, width, and position of each fin as variables; and the area of fins as constraint. The effects of the thermal conductivity of fins, the area of fins, and the number of fins on the optimal structure of fins were discussed. The following conclusions can be made:

- (1) A single fin inserted in the half-ring region should be placed in the lower half due to the effects of natural convection. The optimal dimensionless fin angle,  $\psi$ , is about 0.2, and the optimal dimensionless fin length,  $L$ , is about 0.96. The use of optimal fins can shorten the dimensionless total melting time,  $Fo_{tot}$ , by 68% compared with the case of no fin, and 61.3% compared with uniformly arranged single fin.
- (2) Enlarging fin area will increase the optimal  $\psi$  and decrease the optimal  $L$  when the fin area is added. Nevertheless, the fin area is not a sensitive parameter that affects the optimal position and structure of the fin. When the value of  $A$  is increased by four times, the optimal values of  $L$  and  $\psi$  only change by 10.6% and 9.6%, respectively.
- (3) Thermal conductivity is also not a sensitive parameter for the optimal position and structure of the fin since the area of the fin is limited. As the value of  $\lambda_{fin}/\lambda_{PCM}$  increases from 83.6 to 1987.7, the optimal values of  $L$  and  $\psi$  are only increased by 14.7% and 11%, respectively.
- (4) The number of fins sensitively affects the optimal position and structure of the fins. When the number of fins exceeds one, fins should have respective structural parameters, as well as non-uniform arrangements for effective utilization of natural convection. The advantage of non-uniform fins decreases as the number of fins increases. When the number of fins is four, using the optimized fins can only reduce the  $Fo_{tot}$  by 15.9% compared with using the uniformly arranged fins.

**Author Contributions:** Conceptualization, Z.-J.Z.; data curation, C.H.; formal analysis, C.H.; investigation, Y.X.; methodology, H.Y.; project administration, Z.-J.Z.; software, H.Y.; validation, Y.W.; visualization, M.C.; writing—original draft, Y.X. All authors have read and agreed to the published version of the manuscript.

**Funding:** This research was funded by the National Natural Science Foundation of China (No. 52176215).

**Conflicts of Interest:** The authors declare no conflict of interest.

## Nomenclature

$A$	dimensionless fin area
$A_{\text{mush}}$	mushy zone constant ( $\text{kg m}^{-3} \text{s}$ )
$c_p$	specific heat ( $\text{J kg}^{-1} \text{K}^{-1}$ )
$D$	diameter (m)
$D_e$	hydraulic diameter (m)
$f$	melting fraction
$ Fo$	Fourier number
$g$	acceleration of gravity ( $\text{m s}^{-2}$ )
$\Delta h$	latent heat of fusion ( $\text{kJ kg}^{-1}$ )
$K$	permeability ( $\text{m}^2$ )
$l$	fin length (m)
$L$	dimensionless fin length
$p$	pressure (Pa)
$r$	radius (m)
$Ra$	Rayleigh number
$Ste$	Stefan number
$t$	time (s)
$T$	temperature (K)
$u, v$	x and r velocity components ( $\text{m s}^{-1}$ )
$w$	fin width (m)
$x, y$	Cartesian coordinates (m)
<i>Abbreviation</i>	
CFD	computational fluid dynamics
FVM	finite volume method
GA	genetic algorithm
HTF	heat-transfer fluid
LHTES	latent heat thermal energy storage
PCM	phase-change material
TES	thermal energy storage
<i>Greek symbols</i>	
$\alpha$	thermal diffusivity ( $\text{m}^2 \text{s}^{-1}$ )
$\beta$	thermal expansion coefficient ( $\text{K}^{-1}$ )
$\delta$	small constant number with a value of 0.001
$\Delta$	dimensionless fin width
$\varepsilon$	integer with a value of 0 or 1
$\theta$	angle (rad)
$\lambda$	thermal conductivity ( $\text{W m}^{-1} \text{K}^{-1}$ )
$\mu$	kinetic viscosity ( $\text{kg m}^{-1} \text{s}^{-1}$ )
$\pi$	ratio of the circumference to the diameter of a circle
$\rho$	density ( $\text{kg m}^{-3}$ )
$\Psi$	dimensionless angle

*subscripts*

ave	average
i	inner tube
m	melting
o	outer tube
ref	reference
s	solidification
tot	total
w	wall

**References**

- Guo, J.; Du, Z.; Liu, G.; Yang, X.; Li, M.-J. Compression effect of metal foam on melting phase change in a shell-and-tube unit. *Appl. Therm. Eng.* **2022**, *206*, 118124. [[CrossRef](#)]
- Mosaffa, A.H.; Talati, F.; Basirat Tabrizi, H.; Rosen, M.A. Analytical modeling of PCM solidification in a shell and tube finned thermal storage for air conditioning systems. *Energy Build.* **2012**, *49*, 356–361. [[CrossRef](#)]
- Huang, X.; Yao, S.; Yang, X.; Zhou, R.; Luo, J.; Shen, X. Comparison of solidification performance enhancement strategies for a triplex-tube thermal energy storage system. *Appl. Therm. Eng.* **2022**, *204*, 117997. [[CrossRef](#)]
- Chen, D.; Riaz, A.; Aute, V.C.; Radermacher, R. A solid–liquid model based on lattice Boltzmann method for phase change material melting with porous media in cylindrical heat exchangers. *Appl. Therm. Eng.* **2022**, *207*, 118080. [[CrossRef](#)]
- Liu, Z.; Wang, Z.; Li, P.; Qin, H.; Heng, W. Multi-parameter heat transfer analysis of molten PCM in an inclined enclosure. *Appl. Therm. Eng.* **2022**, *208*, 118209. [[CrossRef](#)]
- Zhang, S.; Pu, L.; Xu, L.; Dai, M. Study on dominant heat transfer mechanism in vertical smooth/finned-tube thermal energy storage during charging process. *Appl. Therm. Eng.* **2022**, *204*, 117935. [[CrossRef](#)]
- Behi, H.; Behi, M.; Ghanbarpour, A.; Karimi, D.; Azad, A.; Ghanbarpour, M.; Behnia, M. Enhancement of the Thermal Energy Storage Using Heat-Pipe-Assisted Phase Change Material. *Energies* **2021**, *14*, 6176. [[CrossRef](#)]
- Yang, C.; Xu, Y.; Cai, X.; Zheng, Z.-J. Effect of the circumferential and radial graded metal foam on horizontal shell-and-tube latent heat thermal energy storage unit. *Sol. Energy* **2021**, *226*, 225–235. [[CrossRef](#)]
- Tselepi, M.; Prouskas, C.; Papageorgiou, D.G.; Lagaris, I.E.; Evangelakis, G.A. Graphene-Based Phase Change Composite Nano-Materials for Thermal Storage Applications. *Energies* **2022**, *15*, 1192. [[CrossRef](#)]
- Karimi, D.; Behi, H.; Van Mierlo, J.; Berecibar, M. An Experimental Study on Thermal Performance of Graphite-Based Phase-Change Materials for High-Power Batteries. *Energies* **2022**, *15*, 2515. [[CrossRef](#)]
- Eslamnezhad, H.; Rahimi, A.B. Enhance heat transfer for phase-change materials in triplex tube heat exchanger with selected arrangements of fins. *Appl. Therm. Eng.* **2017**, *113*, 813–821. [[CrossRef](#)]
- Kalhari, B.; Ramadhyani, S. Studies on heat transfer from a vertical cylinder, with or without fins, embedded in a solid phase change medium. *J. Heat Transf.* **1985**, *107*, 44–51. [[CrossRef](#)]
- Rabienataj Darzi, A.A.; Jourabian, M.; Farhadi, M. Melting and solidification of PCM enhanced by radial conductive fins and nanoparticles in cylindrical annulus. *Energy Convers. Manag.* **2016**, *118*, 253–263. [[CrossRef](#)]
- Agyenim, F.; Eames, P.; Smyth, M. A comparison of heat transfer enhancement in a medium temperature thermal energy storage heat exchanger using fins. *Sol. Energy* **2009**, *83*, 1509–1520. [[CrossRef](#)]
- Li, Z.; Wu, Z.-G. Analysis of HTFs, PCMs and fins effects on the thermal performance of shell–tube thermal energy storage units. *Sol. Energy* **2015**, *122*, 382–395. [[CrossRef](#)]
- Rozenfeld, T.; Kozak, Y.; Hayat, R.; Ziskind, G. Close-contact melting in a horizontal cylindrical enclosure with longitudinal plate fins: Demonstration, modeling and application to thermal storage. *Int. J. Heat Mass Transf.* **2015**, *86*, 465–477. [[CrossRef](#)]
- Padmanabhan, P.V.; Krishna Murthy, M.V. Outward phase change in a cylindrical annulus with axial fins on the inner tube. *Int. J. Heat Mass Transf.* **1986**, *29*, 1855–1868. [[CrossRef](#)]
- Ismail, K.A.R.; Alves, C.L.F.; Modesto, M.S. Numerical and experimental study on the solidification of PCM around a vertical axially finned isothermal cylinder. *Appl. Therm. Eng.* **2001**, *21*, 53–77. [[CrossRef](#)]
- Zhang, C.; Sun, Q.; Chen, Y. Solidification behaviors and parametric optimization of finned shell-tube ice storage units. *Int. J. Heat Mass Transf.* **2020**, *146*, 118836. [[CrossRef](#)]
- Hosseini, M.J.; Ranjbar, A.A.; Rahimi, M.; Bahrampoury, R. Experimental and numerical evaluation of longitudinally finned latent heat thermal storage systems. *Energy Build.* **2015**, *99*, 263–272. [[CrossRef](#)]
- Solomon, G.R.; Velraj, R. Analysis of the heat transfer mechanisms during energy storage in a Phase Change Material filled vertical finned cylindrical unit for free cooling application. *Energy Convers. Manag.* **2013**, *75*, 466–473. [[CrossRef](#)]
- Yuan, Y.; Cao, X.; Xiang, B.; Du, Y. Effect of installation angle of fins on melting characteristics of annular unit for latent heat thermal energy storage. *Sol. Energy* **2016**, *136*, 365–378. [[CrossRef](#)]
- Abhat, A.; Aboul-Enein, S.; Malatidis, N.A. Heat-of-fusion storage systems for solar heating applications. In *Thermal Storage of Solar Energy*; Springer: Dordrecht, The Netherlands, 1981; pp. 157–171.
- Bathelt, A.G.; Viskanta, R. Heat transfer and interface motion during melting and solidification around a finned heat source/sink. *J. Heat Transf.* **1981**, *103*, 720–726. [[CrossRef](#)]

25. Sparrow, E.M.; Larson, E.D.; Ramsey, J.W. Freezing on a finned tube for either conduction-controlled or natural-convection-controlled heat transfer. *Int. J. Heat Mass Transf.* **1981**, *24*, 273–284. [[CrossRef](#)]
26. Rathod, M.K.; Banerjee, J. Thermal performance enhancement of shell and tube Latent Heat Storage Unit using longitudinal fins. *Appl. Therm. Eng.* **2015**, *75*, 1084–1092. [[CrossRef](#)]
27. Dhaidan, N.S.; Khodadadi, J.M. Improved performance of latent heat energy storage systems utilizing high thermal conductivity fins: A review. *J. Renew. Sustain. Energy* **2017**, *9*, 034103. [[CrossRef](#)]
28. Wang, P.; Yao, H.; Lan, Z.; Peng, Z.; Huang, Y.; Ding, Y. Numerical investigation of PCM melting process in sleeve tube with internal fins. *Energy Convers. Manag.* **2016**, *110*, 428–435. [[CrossRef](#)]
29. Mahood, H.B.; Mahdi, M.S.; Monjezi, A.A.; Khadom, A.A.; Campbell, A.N. Numerical investigation on the effect of fin design on the melting of phase change material in a horizontal shell and tube thermal energy storage. *J. Energy Storage* **2020**, *29*, 101331. [[CrossRef](#)]
30. Tao, Y.B.; He, Y.L. Effects of natural convection on latent heat storage performance of salt in a horizontal concentric tube. *Appl. Energy* **2015**, *143*, 38–46. [[CrossRef](#)]
31. Deng, S.; Nie, C.; Wei, G.; Ye, W.-B. Improving the melting performance of a horizontal shell-tube latent-heat thermal energy storage unit using local enhanced finned tube. *Energy Build.* **2019**, *183*, 161–173. [[CrossRef](#)]
32. Deng, S.; Nie, C.; Jiang, H.; Ye, W.-B. Evaluation and optimization of thermal performance for a finned double tube latent heat thermal energy storage. *Int. J. Heat Mass Transf.* **2019**, *130*, 532–544. [[CrossRef](#)]
33. Kumar, R.; Verma, P. An experimental and numerical study on effect of longitudinal finned tube eccentric configuration on melting behaviour of lauric acid in a horizontal tube-in-shell storage unit. *J. Energy Storage* **2020**, *30*, 101396. [[CrossRef](#)]
34. Yagci, O.K.; Avci, M.; Aydin, O. Melting and solidification of PCM in a tube-in-shell unit: Effect of fin edge lengths' ratio. *J. Energy Storage* **2019**, *24*, 100802. [[CrossRef](#)]
35. Mao, Q.; Hu, X.; Zhu, Y. Numerical Investigation of Heat Transfer Performance and Structural Optimization of Fan-Shaped Finned Tube Heat Exchanger. *Energies* **2022**, *15*, 5682. [[CrossRef](#)]
36. Sun, X.; Mahdi, J.M.; Mohammed, H.I.; Majdi, H.S.; Zixiong, W.; Talebizadehsardari, P. Solidification Enhancement in a Triple-Tube Latent Heat Energy Storage System Using Twisted Fins. *Energies* **2021**, *14*, 7179. [[CrossRef](#)]
37. Chen, Q.; Wu, J.; Sun, K.; Zhang, Y. Numerical Study of Heat Transfer Enhancement by Arc-Shaped Fins in a Shell-Tube Thermal Energy Storage Unit. *Energies* **2022**, *15*, 7799. [[CrossRef](#)]
38. Abdulateef, A.M.; Mat, S.; Abdulateef, J.; Sopian, K.; Al-Abidi, A.A. Geometric and design parameters of fins employed for enhancing thermal energy storage systems: A review. *Renew. Sustain. Energy Rev.* **2018**, *82 Pt 1*, 1620–1635. [[CrossRef](#)]
39. Cai, X.; Zheng, Z.-J.; Yang, C.; Xu, Y. Improving the solidification performance of a shell-and-tube latent-heat thermal energy storage unit using a connected-Y-shaped fin. *Int. J. Energy Res.* **2022**, *46*, 12758–12771. [[CrossRef](#)]
40. Xu, Y.; Li, M.J.; Zheng, Z.J.; Xue, X.D. Melting performance enhancement of phase change material by a limited amount of metal foam: Configurational optimization and economic assessment. *Appl. Energy* **2018**, *212*, 868–880. [[CrossRef](#)]
41. Xu, Y.; Ren, Q.L.; Zheng, Z.J.; He, Y.L. Evaluation and optimization of melting performance for a latent heat thermal energy storage unit partially filled with porous media. *Appl. Energy* **2017**, *193*, 84–95. [[CrossRef](#)]
42. Zheng, Z.J.; Xu, Y.; Li, M.J. Eccentricity optimization of a horizontal shell-and-tube latent-heat thermal energy storage unit based on melting and melting-solidifying performance. *Appl. Energy* **2018**, *220*, 447–454. [[CrossRef](#)]
43. Xu, Y.; Zheng, Z.-J.; Chen, S.; Cai, X.; Yang, C. Parameter analysis and fast prediction of the optimum eccentricity for a latent heat thermal energy storage unit with phase change material enhanced by porous medium. *Appl. Therm. Eng.* **2021**, *186*, 116485. [[CrossRef](#)]
44. Zheng, Z.-J.; Cai, X.; Yang, C.; Xu, Y. Improving the solidification performance of a latent heat thermal energy storage unit using arrow-shaped fins obtained by an innovative fast optimization algorithm. *Renew. Energy* **2022**, *195*, 566–577. [[CrossRef](#)]
45. Zheng, Z.-J.; Yang, C.; Xu, Y.; Cai, X. Effect of metal foam with two-dimensional porosity gradient on melting behavior in a rectangular cavity. *Renew. Energy* **2021**, *172*, 802–815. [[CrossRef](#)]
46. Zheng, Z.J.; Li, M.J.; He, Y.L. Optimization of porous insert configurations for heat transfer enhancement in tubes based on genetic algorithm and CFD. *Int. J. Heat Mass Transf.* **2015**, *87*, 376–379. [[CrossRef](#)]
47. Zheng, Z.J.; He, Y.; He, Y.L.; Wang, K. Numerical optimization of catalyst configurations in a solar parabolic trough receiver-reactor with non-uniform heat flux. *Sol. Energy* **2015**, *122*, 113–125. [[CrossRef](#)]
48. Zheng, Z.J.; Li, M.J.; He, Y.L. Thermal analysis of solar central receiver tube with porous inserts and non-uniform heat flux. *Appl. Energy* **2017**, *185*, 1152–1161. [[CrossRef](#)]
49. Zheng, Z.J.; Xu, Y.; He, Y.L. Study on the performance of a shell-and-tube latent-heat storage unit enhanced by porous medium with graded porosity (in chinese). *J. Eng. Thermophys.* **2019**, *40*, 129–135.
50. Xu, Y.; Zheng, Z.J.; Li, M.J. A half-analytical correlation of total melting time for shell-and-tube latent-heat thermal energy storage unit. *Appl. Therm. Eng.* **2019**, *161*, 114176. [[CrossRef](#)]
51. Xu, Y.; Zheng, Z.J.; Yang, C.; Cai, X. Intelligent optimization of horizontal fins to improve the melting performance of phase change materials in a square cavity with isothermal vertical wall. *J. Energy Storage* **2021**, *44*, 103334. [[CrossRef](#)]
52. Zheng, Z.J.; Xu, Y.; He, Y.L. Thermal analysis of a solar parabolic trough receiver tube with porous insert optimized by coupling genetic algorithm and CFD. *Sci. China Technol. Sci.* **2016**, *59*, 1475–1485. [[CrossRef](#)]